Int. J. Electrochem. Sci., 15 **(2020)** 765 – 773, doi: 10.20964/2020.01.65

International Journal of
ELECTROCHEMICAL
SCIENCE
www.electrochemsci.org

A Facile Synthesis of ZnO Nanorods on Nitrogen-Doped Graphene Sheets for Supercapacitor Applications

Jianping Xu, Jie Huang, Meiwu Zhu, Chuanhong Cheng, Tianxiang Jin[*], *Bin Huang*[*]

Jiangxi Key Laboratory for Mass Spectrometry and Instrumentation, East China University of Technology, Nanchang 344000, P.R. China
[*]E-mail: binhuang_ecit@163.com, sphinxjtx@ecit.edu.cn

Received: 8 September 2019 / *Accepted:* 8 November 2019 / *Published:* 30 November 2019

ZnO nanorods/nitrogen-doped graphene (ZnO@NG) composite networks were prepared by a convenient hydrothermal method from zinc acetate and graphene oxide (GO) using ethylene glycol as the reducing agent. ZnO nanorods were observed to be homogeneously supported on the NG networks with a length and diameter of 1–2 μm and 50–100 nm, respectively. High specific capacity (237.18 F/g, 0.5 A/g) can be obtained by integrating porous NG networks and ZnO nanorods as ultracapacitance electrodes. ZnO@NG also exhibits an excellent electrochemical stability of 90.8% for 2000 cycles at 0.5 A/g. In this study, a new method is proposed for the preparation of heteroatom-doped graphene and metal oxide composite for high-performance supercapacitors.

Keywords: nitrogen-doped graphene (NG), ZnO@NG, supercapacitor, solvothermal method

1. INTRODUCTION

The demand for environment-friendly and sustainable energy resources has been increasing due to the depletion of traditional fossil fuels and related ecological problems [1]. Therefore, it is essential to conduct in-depth studies on advanced energy storage devices. Among all types of energy storage devices, supercapacitors (SCs) have drawn increasingly more attention because of their high power density, high charging and discharging speed, and long cycling life [2, 3].

Carbon-based materials such as graphene are ideal materials for electrodes because of their large specific surface area and high electron conductivity [4–6]. Moreover, the incorporation of heteroatoms such as nitrogen, boron, iodine, sulfur, and phosphorus into graphene sheets is effective for improving the capacitive performance of electrodes because of the formation of active sites in electrochemical process [7, 8]. Besides, the incorporation of heteroatoms into carbon lattices can enhance the charge density and electrode wettability, thus boosting the capacitive performance.

However, because of the agglomeration of graphene, its specific surface area is relatively low, which is not conducive to obtain a high specific capacitance (Cs) [9]. In view of this shortcoming, transition-metal oxides (TMOs) can be introduced into the system to fabricate hybrid capacitors, because TMOs can greatly enhance the Cs and energy density of carbon-based electrodes [10, 11].

TMOs including MnO_2, Co_3O_4, Fe_2O_3, SnO_2, and CuO are low cost, high electroactive, and environment-friendly pseudocapacitor materials [12–16]. Nowadays, zinc and its compounds are extensively applied in electrochemical sensors, capacitors, and organic chemical catalysts [17–19]. Among the existing TMOs, ZnO is one of the most widely used materials because of its simple synthesis, diverse morphology, and high electrochemical activity. ZnO can be used as an electrochemical active material, and its energy density can reach 650 Wh/g [20].

Although studies are reported on the use of ZnO/carbon as SC electrode, the synthesis of ZnO/carbon is still rigorous, and its Cs is relatively low. To solve these problems, we propose a convenient strategy to fabricate ZnO/nitrogen-doped graphene nanocomposites as SC electrodes. The nanocomposites were prepared using a simple hydrothermal method, and their morphologies were characterized by SEM and XRD analyses. The morphologies of nanocomposites showed that ZnO nanorods are efficiently fixed on the surface of NG. SC electrodes were fabricated from these nanocomposite materials. The electrochemical measurements show that the performance of as-prepared hybrid ZnO@NG electrodes is much better than that of electrodes composed of a single component. Considering the convenient fabrication procedure and excellent synergistic effect, the ZnO@NG electrode material is a potential candidate for high-performance SCs.

2. EXPERIMENTAL

2.1. Chemicals

Zinc nitrate hexahydrate, urea, and ethylene glycol were obtained from Sigma-Aldrich. $KMnO_4$, KOH, $NaNO_3$, 98% H_2SO_4, 30% H_2O_2, and graphite powder were obtained from China Medicine Co. All the reagents were of analytical grade.

2.2. Preparation of ZnO@NG

Graphene oxide (GO) was synthesized using a modified Hummer's method [21,22] using graphite powder as the starting material. First, 10 mg GO, 20 mg zinc nitrate hexahydrate, and 10 mg urea were mixed in 50 mL distilled water. Then, 10 mL ethylene glycol was dropped into the stirred solution to obtain a gray slurry. After 60 min of stirring, the mixture was moved into a 200-mL Teflon-lined autoclave and kept at 150 °C overnight. After being cooled to 20–30 °C, the final mixture was centrifuged and washed with deionized water and ethanol repeatedly and dried at 60 °C for 24 h. Finally, the solid sample was heated at 800 °C for 3 h under argon flow. For comparison, the NG was prepared in the absence of zinc nitrate hexahydrate, and free ZnO was prepared in the absence of GO and urea following the same procedure.

2.3. Electrochemical Characterization

All the electrochemical measurements were performed using a CHI 660E electrochemical cell equipped with a 3-electrode system in a 6 M KOH solution. A saturated calomel electrode (SCE) and Pt wire served as the reference and counter electrodes, respectively. The working electrode was fabricated by mixing the as-prepared nanomaterials (85 wt%) with PTFE (5 wt%) and carbon black (CB, 10 wt%) and then pressed onto a Ni foam (1 cm × 1.5 cm) and dried under vacuum. The electrochemical properties of ZnO@NG electrode were tested by cyclic voltammetry (CV) and galvanostatic charging/discharging (GCD) techniques. The Cs was calculated from the GCD curves using Eq. (1).

$$C = \frac{I \cdot t}{m \cdot \Delta U} \qquad (1)$$

where I is the discharge current, t is the discharge time, m is the mass of ZnO@NG composites, and ΔU is the voltage window (here, $\Delta U = 1.0$ V).

2.4. Characterization of materials

SEM observation was performed using a field-emission SEM (FE-SEM, Hitachi S-4800) at 5–10 kV. The structure of materials was investigated by XRD analysis (Shimadzu, X-6000, Cu Kα radiation). XPS analyses were performed using a Thermo Fisher X-ray photoelectron spectrometer (Al Kα radiation).

3. RESULTS AND DISCUSSION

3.1. Morphologies and Structure of NG and ZnO@NG

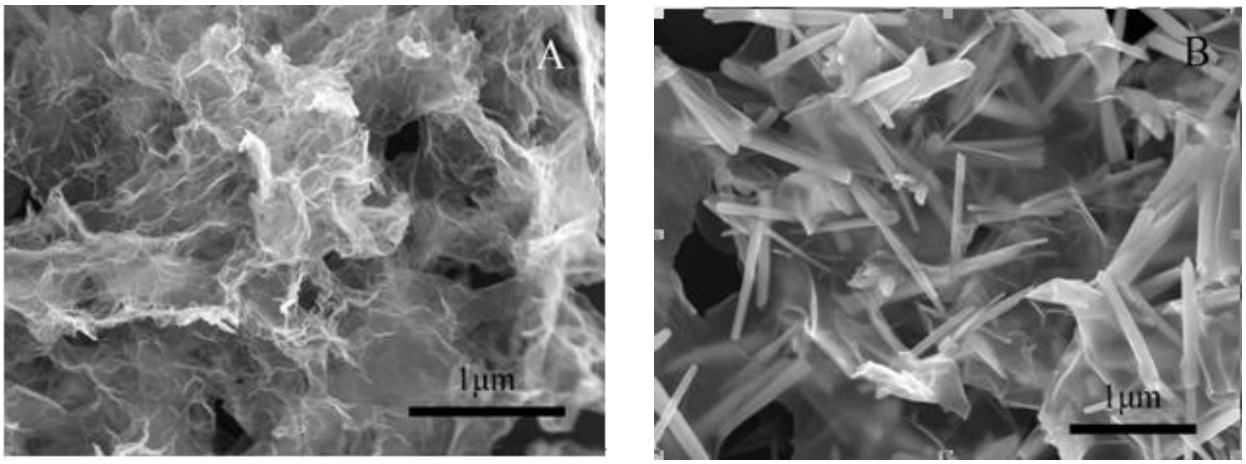

Figure 1. SEM images of NG (A) and ZnO@NG (B)

The micromorphology of as-prepared NG was observed by SEM, as shown in Fig. 1A. The NG

exhibits a fluffy, distinct crumpled, and highly porous three-dimensional (3D) network structure with pore sizes ranging from submicron to several microns. The NG nanosheets are randomly stacked and compact, exhibiting a laminar feature like crumpled silk or veil. This morphology can be assigned to the defective structures caused by the nitrogen dopant atoms.

Fig. 1B shows that ZnO nanorods were uniformly supported on the porous network of NG. The diameters of individual rods are in the range of 50–100 nm, and their lengths are 1–2 μm. The ZnO nanorods act as spacers between graphene sheets to prevent their stacking. This ensures a high specific surface area of the electrode material, providing more electroactive sites for the Faradic reaction and improving the ion diffusion rate.

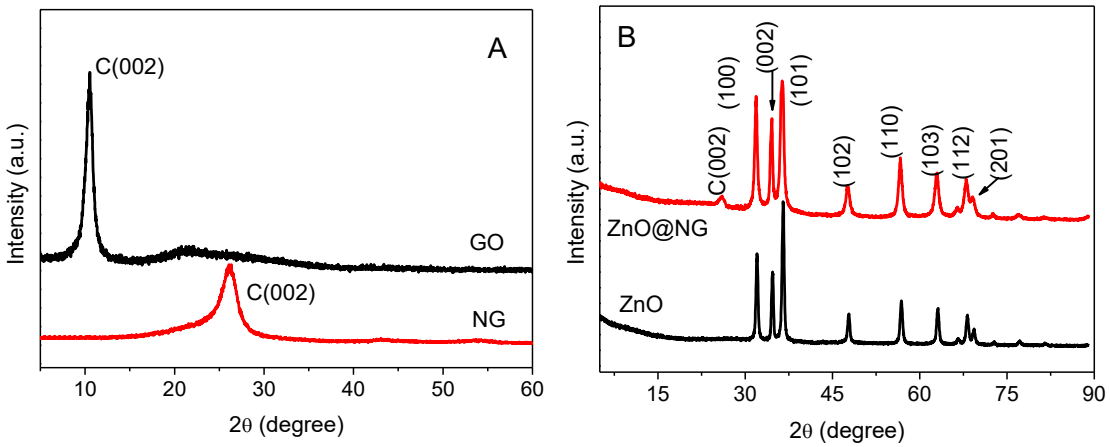

Figure 2. XRD patterns: (A) GO and NG, (B) free ZnO and ZnO@NG.

The structures of as-obtained GO and NG were analyzed by XRD, as shown in Fig. 2A. The GO pattern shows a single sharp diffraction peak centered at 10.4° corresponding to an interlayer distance of 0.80 nm, indicating the complete oxidation of graphite to GO. NG exhibited a broad peak C (002) at ~26.2° corresponding to an interlayer space of ~0.34 nm. The interlayer space of NG decreased, because the oxygen-based functional groups on the basal plane of GO were removed. Fig. 2B shows the XRD patterns of free ZnO and ZnO@NG composite. The diffraction peaks of ZnO are consistent with the hexagonal wurtzite structure (JCPDS NO. 01-080-0075) for both pristine and composite samples. The nano-ZnO crystal phase was observed at 31.7°, 34.4°, 36.2°, 47.4°, 56.5°, and 62.9°, corresponding to the (100), (002), (101), (102), (110), and (103) planes. Besides, a small peak appeared at 26.2°, corresponding to the (002) plane of NG. The small and weak C (002) peak was caused by the low amount and low diffraction intensity of NG.

The relevant structural modification, chemical composition, and doped-bonding configurations of ZnO@NG were characterized by XPS analyses (Fig. 3). The peaks of XPS survey spectrum at ~285, 400, 532, and 1022–1045 eV correspond to the carbon, nitrogen, oxygen, and zinc elements, respectively. The high-resolution XPS spectrum of Zn2p (Fig. 3A$_1$) exhibited two strong peaks at 1021.80 and 1044.95 eV, corresponding to $Zn2p^{3/2}$ and $Zn2p^{1/2}$, respectively[23].

The high-resolution N 1s spectrum of composites is shown in Fig. 3B. N 1s spectrum was fitted

with three different component peaks, corresponding to pyridinic-N (398.2 eV), pyrrolic-N (399.8 eV), and graphitic-N (401 eV), consistent with other N-doped carbon materials. As expected, a large proportion of pyrrolic-N and pyridinic-N within ZnO@NG are beneficial for boosting pseudocapacitance by redox reactions, while graphitic-N can improve the electroconductivity of carbon-based materials [24].

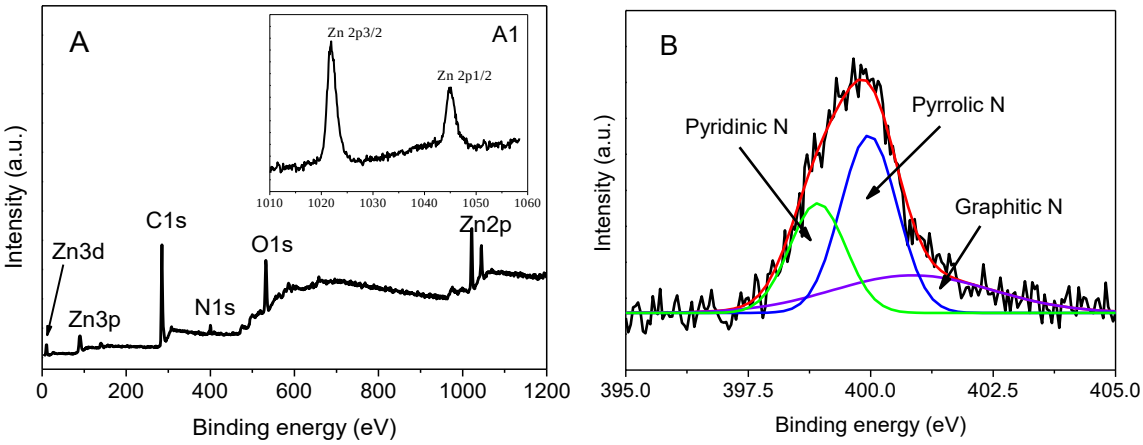

Figure 3. (A) XPS survey spectra of ZnO@NG, (A1) high-resolution XPS spectra of Zn2p region and (B) N 1s region.

3.2. Electrochemical Performance

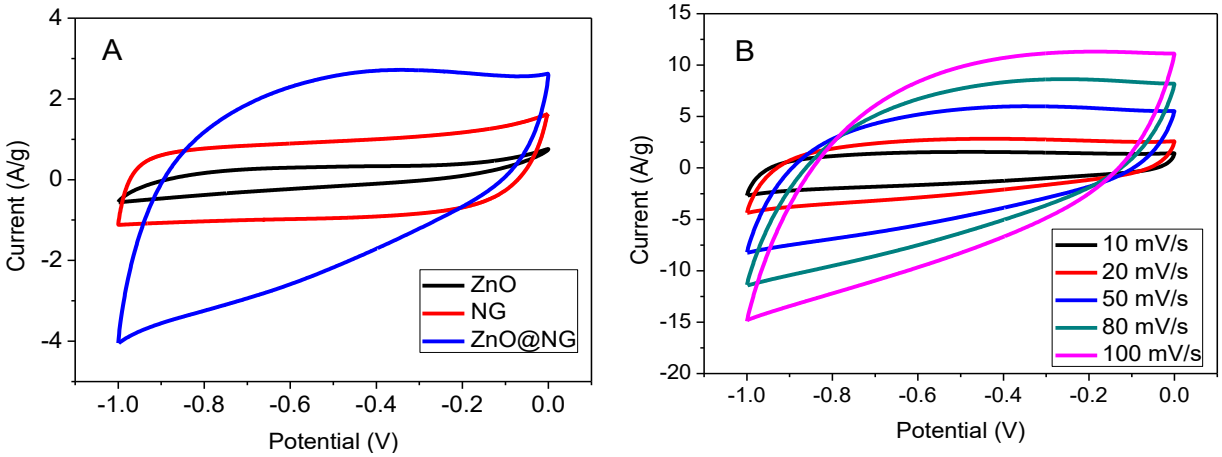

Figure 4. (A) CV curves of ZnO nanorods, NG and ZnO@NG measured at a scan rate of 20 mV/s. (B) CV profiles of ZnO@NG measured at different scan rates of 10–100 mV/s.

The electrochemical properties of ZnO nanorods, NG, and ZnO@NG composites are shown in Fig. 4A. The ZnO@NG electrode exhibits a larger enclosed area in the CV curves, indicating that the capacitance of ZnO@NG materials is much higher than that of free ZnO nanorods and NG [25]. This can be attributed to the high electrochemical capacity of coated ZnO nanorods because of its reversible redox reaction, which is crucial to obtain good electrochemical performance [26]. Figure 4B shows the CV profiles of ZnO@NG composite in the potential range 0.0−1.0 V at a sweep speed of 10−100 mV/s.

The shapes of CV have near-rectangular characteristics, indicating that the materials have excellent capacitive behavior. With an increase in sweep speed, the current response increases accordingly. Moreover, the CV profiles remain quasi-rectangular at a high scan rate of 100 mV/s without drastic change, indicating a good rate performance.

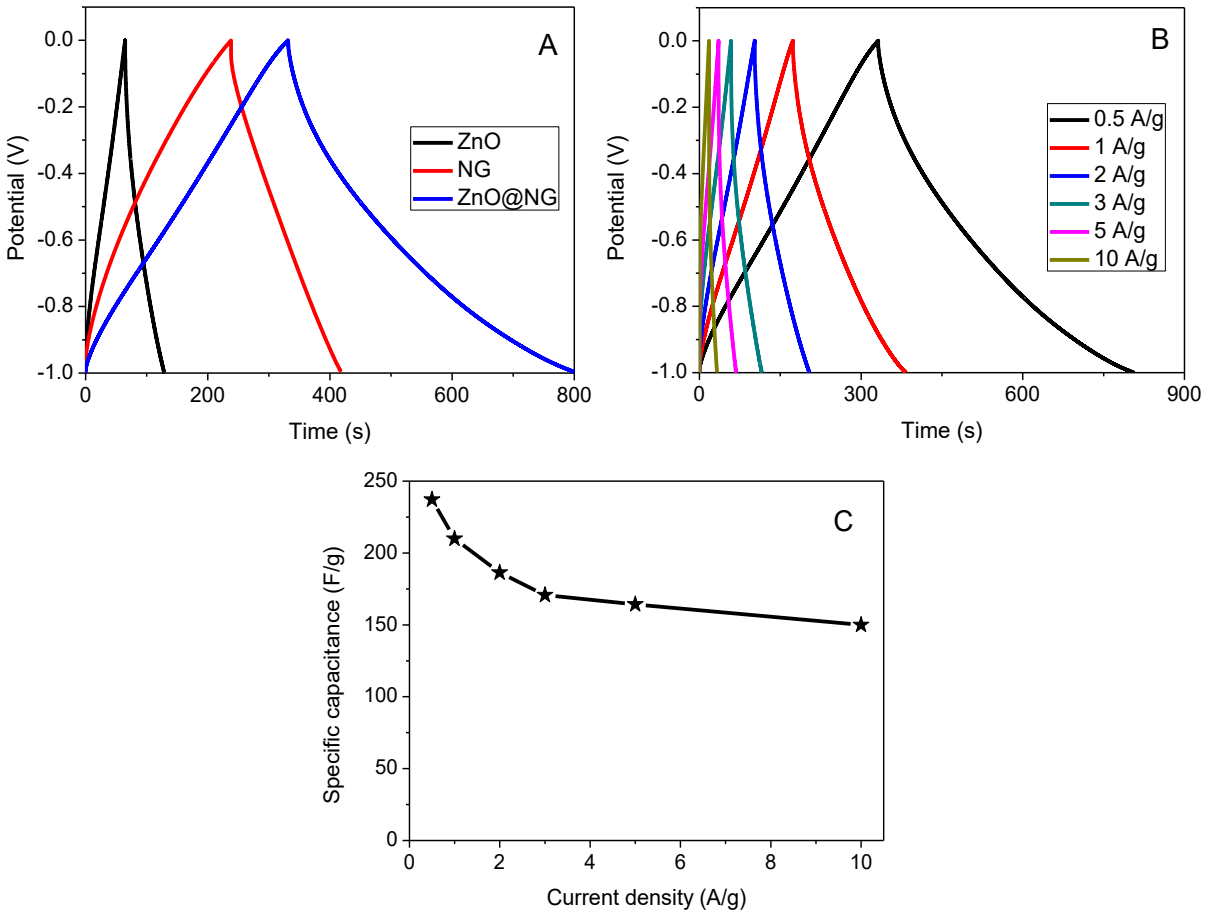

Figure 5. (A) GCD curves of free ZnO nanorods, NG, and ZnO@NG at 0.5 A/g. (B) GCD curves of ZnO@NG at various current densities from 0.5 to 10 A/g, (C) Cs calculated from GCD curves.

The GCD curves of free ZnO nanorods, NG, and ZnO@NG electrodes were measured at 0.5 A/g, as shown in Fig. 5A. The three curves have an isosceles triangle shape. The Cs of ZnO@NG (237.18 F/g) is much larger than those of NG (91.10 F/g) and free ZnO (31.75 F/g) at the same current density. The integration of graphene and ZnO could effectively enhance the overall Cs comparing with pristine metal oxides and NG[26]. The enhancement of capacitive performance of ZnO@NG composites can certainly be attributed to two aspects: (1) NG is used as a highly conductive network in the nanocomposites; this is beneficial for fast electron transport and eventually leads to better electrochemical properties. (2) ZnO nanorods, which are electrochemically active sites with a high surface area, induce the surface Faradic process as follows:

$$ZnO + OH^- \rightleftharpoons ZnOOH + e^-$$

For more details, GCD tests of ZnO@NG hybrids were carried out (Fig. 5B). The linear and symmetrical curves at different current densities from 0.5 to 10 A/g are demonstrated within a potential window of −1.0 to 0 V, indicating stable electrochemical reversibility. Based on the GCD curves, the values of Cs at different current densities were calculated using Eq. (1)

As expected, the current density increases with the slight decrease in Cs value. This is because the ion-accessible electroactive surface area decreases when the scan rate increases. The Cs of as-prepared ZnO@NG hybrids can reach up to 237.18 F/g at 0.5 A/g, and it also exhibits an admirable rate capability (150 F/g retained at 10 A/g).

Long electrochemical cycle life is a crucial requirement in the daily application of electrode materials for energy storage devices. A cycle stability measurement was carried out by generating 2000 continuous CV cycling for ZnO@NG; the variation in Cs as a function of cycle number is shown in Fig. 6. The inset presents the CV plots of the first cycle and the 2000th cycle. The Cs of ZnO@NG is maintained at 215.36 F/g with 90.8% retention after 2000 cycles. Besides, almost no obvious change was observed between the CV plots before and after the long-term cycling measurement (inset of Fig. 6), indicating an outstanding cycle stability performance.

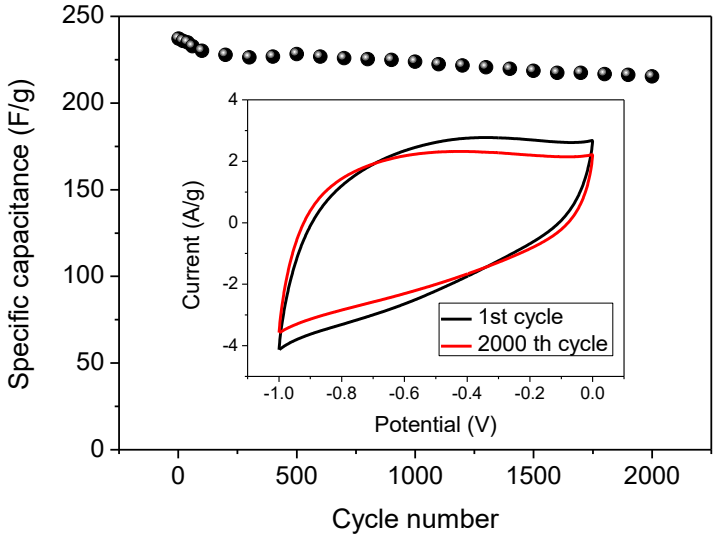

Figure 6. Cycle stability of ZnO@NG electrode in 6 M KOH electrolyte.

In addition, we further compared the as-prepared electrode material with other ZnO-based materials in literature; the results are shown in Table 1. Obviously, the ZnO@NG electrode reported in this study exhibits a higher Cs than other ZnO-based materials. The ZnO@NG electrode materials have good electrochemical properties; this can be ascribed to three aspects: First, the hierarchical structures favor the rapid diffusion of electrolyte ions throughout the ZnO@NG electrodes. Second, the NG serves as a matrix with excellent electroconductivity and specific surface area to ensure fast Faradaic reactions of ZnO nanorods. Finally, the ZnO nanorod is used as spacers to prevent NG from agglomeration. This structure can provide more inner active sites that contribute to the Cs [34].

Table 1. Partial list of reported carbon-based materials for Cs

ZnO-based materials	Electrolyte	C_s (F/g)	Reference
Boron-doped ZnO/RGO	6 M KOH	230.50 (5 mV/s)	[25]
Graphene-ZnO	6 M KOH	122.4 (5 mV/s)	[26]
ZnO nanoflowers/rGO	3.5 M KOH	203 (1 A/g)	[27]
Sandwich-type ZnO/rGO/ZnO	1 M KCl	60.63 (5 mV/s)	[28]
ZnO/activated carbon	1 M Na_2SO_4	155 (0.5A/g)	[29]
ZnO-Au nanocomposites	2 M KOH	205 (20 mV/s)	[29]
ZnO flowers	2 M KOH	89 (20 mV/s)	[30]
ZnO/RGO composite	1 M Na_2SO_4	60.2 (10 mV/s)	[31]
ZnO@NG	6 M KOH	237.18 (0.5 A/g)	this study

RGO or rGO: Chemically-reduced graphene oxide

4. CONCLUSIONS

In this study, we successfully fabricated ZnO nanorods/NG composite networks using a simple hydrothermal process. ZnO nanorods were supported on NG networks homogeneously with a length and diameter of 1–2 μm and 50–100 nm, respectively. The as-obtained ZnO@NG composite exhibits excellent electrochemical performance including a high Cs (237.18 F/g at a current density of 0.5 A/g), good rate capability (150 F/g retained at a high current density of 10 A/g), and long-term stability (90.8% of the initial capacitance remained after 2000 charge/discharge cycles). This study could open a new way to fabricate heteroatom-doped graphene and metal oxide composites for high-performance SC applications.

ACKNOWLEDGEMENTS
This work was jointly supported by the NSFC (41562021), the Open Project Program of Jiangxi Key Laboratory for Mass Spectrometry and Instrumentation (JXMS201611), NSF of Jiangxi Province (20171BAB206016 and 20161BAB204191), and the Foundation of Jiangxi Educational Committee (GJJ160565 and GJJ180365).

References

1. J. Cherusseri, K. S. Kumar, D. Pandey, E. Barrios, J. Thomas, *Small*, 15 (2019) 1902606.
2. X. Tian, J. Jin, S. Yuan, C. K. Chua, S. B. Tor, K. Zhou, *Adv. Energy Mater.*, 7 (2017) 1700127.
3. C. Zhu, T. Liu, F. Qian, T. Y. J. Han, E. B. Duoss, J. D. Kuntz, C. M. Spadaccini, M. A. Worsley, Y. Li, *Nano Lett.*, 16 (2016) 3448.
4. Q. Zhang, K. Scrafford, M. Li, Z. Cao, Z. Xia, P. M. Ajayan, B. Wei, *Nano Lett.*, 14 (2014) 1938.

5. J. Chen, T. Zhu, X. Fu, G. Ren, C. Wang, *Int. J. Electrochem. Sci.*, 14 (2019) 7293.
6. T. Zhu, J. B. Ding, Q. Shao, Y. Qian, X. Q. Huang, *ChemCatChem*, 11 (2019) 689.
7. L. Dai, Y. Xue, L. Qu, H. Choi, J. Baek, *Chemical Reviews*, 115 (2015) 4823.
8. X. Yan, Y. Yu, S. Ryu, J. Lan, X. Yang, *Electrochimica Acta*, 136 (2014) 466.
9. W. Liu, C. Lu, X. Wang, R. Y. Tay, B. K. Tay, *ACS Nano*, 9 (2015) 1528.
10. M. Li, Z. Tang, M. Leng, J. Xue, *Adv. Funct. Mater.*, 24 (2014) 7495.
11. B. Pant, M. Park, G. P. Ojha, J. Park, Y. S. Kuk, E. J. Lee, H. Y. Kim, S. J. Park, *J. Colloid Interface Sci.*, 522 (2018) 40.
12. B. Huang, C. Huang, Y. Qian, *Int. J. Electrochem. Sci.*, 12 (2017) 11171.
13. Y. Zhang, S. J. Park, *J. Mater. Chem. A*, 6 (2018) 20304.
14. Z. Zhai, B. Leng, N. Yang, B. Yang, L. Liu, N. Huang, X. Jiang, *Small*, 15 (2019) 1901527.
15. T. Fan, C. Huang, R. Chen, J. Xu, C. Wang, Y. Qian, *Int. J. Electrochem. Sci.*, 12 (2017) 7659.
16. J. Hao, L. Ji, K. Wu and N. Yang, *Carbon*, 130 (2018) 480.
17. Y. Qian, C. Y. Wang, F. L. Gao, *Biosens. Bioelectron.*, 63 (2015) 425.
18. Y. Qian, C. Y. Wang, F. L. Gao, *Anal. Chim. Acta*, 845 (2014) 1.
19. J. Lortie, T. Dudding, B. M. Gabidullin G. I. Nikonov, *ACS Catal*., 7 (2017) 8454.
20. J. Huang, Z. Yang, B. Yang, R. Wang,T. Wang, *J. Power Sources*, 271 (2014) 143.
21. W. S. Hummers, R. E. Offeman, *J. Am. Chem. Soc.*, 80 (1958) 1339.
22. Y. Qian, F. Ye, J. Xu, *Int. J. Electrochem. Sci.*, 7 (2012) 10063.
23. K. Alali, J. Liu, Q. Liu, R. Li, Z. Li, P. Liu, K. Aljebawi, J. Wang, *RSC Adv.*, 7 (2017) 11428.
24. L. Sun, C. Tian, Y. Fu, J. Yin, L. Wang, H. Fu, *Chem. Eur. J.*, 20 (2014) 564.
25. Ü. Alver, A. Tanriverdi, *Appl. Surf. Sci.*, 378 (2016) 368.
26. M. Saranya, R. Ramachandran, F. Wang, *Journal of Science: Advanced Materials and Devices*, 1 (2016) 454.
27. K. Subramani, M. Sathish, *Mater. Lett.*, 236 (2019) 424.
28. M. Ghorbani, M. Golobostanfard, H. Abdizadeh, *Appl. Surf. Sci.*, 419 (2017) 277.
29. K. Wang, S. Lee, C. W. Park, J-D. Kim, *Colloids and Surfaces A*, 555 (2018) 482.
30. H. Mahajan, J. Bae, K. Yun, *J. Alloys and Comp.*, 758 (2018) 131.
31. Y. Ian, Y. Bu, R, Huang, *Materials Science in Semiconductor Processing*, 31 (2015) 131.